

# GGSD: GENERATING GRAPHS VIA SPECTRAL DIFFUSION

**Anonymous authors**

Paper under double-blind review

## ABSTRACT

In this paper, we present **GGSD**, a novel graph generative model based on 1) the spectral decomposition of the graph Laplacian matrix and 2) a diffusion process. Specifically, we propose to use a denoising model to sample eigenvectors and eigenvalues from which we can reconstruct the graph Laplacian and adjacency matrix. Using the Laplacian spectrum allows us to naturally capture the structural characteristics of the graph and work directly in the node space while avoiding the quadratic complexity bottleneck that limits the applicability of other diffusion-based methods. This, in turn, is accomplished by truncating the spectrum, which, as we show in our experiments, results in a faster yet accurate generative process, and by designing a novel transformer-based architecture linear in the number of nodes. Our permutation invariant model can also handle node features by concatenating them to the eigenvectors of each node. An extensive set of experiments on both synthetic and real-world graphs demonstrates the strengths of our model against state-of-the-art alternatives.

## 1 INTRODUCTION

Generating realistic graphs by learning from a distribution of real-world graphs has gained increasing attention from researchers in many fields due to its wide range of applications. For instance, synthetic graph generation plays a crucial role in drug design Gómez-Bombarelli et al. (2018); Li et al. (2018a); You et al. (2018a) as well as in network science Watts & Strogatz (1998); Leskovec et al. (2010); Albert & Barabási (2002).

**Seminal** graph generation approaches date back to the 1960s and rely on simple stochastic processes, limiting their ability to capture complex dependencies seen in real-world networks. For example, the Barabási-Albert Albert & Barabási (2002) and Kronecker Leskovec et al. (2010) graph models are specifically designed to generate graphs belonging to specific families and lack the ability to learn directly from observed data. While these models may excel in capturing a set of predefined properties, they are often unable to represent a wider range of aspects observed in real-world graphs. In addition, in several domains, network properties are largely unknown, which further limits the applicability of these techniques. For instance, the Barabási-Albert model Albert & Barabási (2002) allows to create graphs that exhibit the scale-free nature found in empirical degree distributions, however it is unable to capture other facets of real-world graphs, *e.g.*, community structure. **While a flurry of new models attempting to address these shortcomings have been introduced by the network science community (see Drobyshevskiy & Turdakov (2019) for a recent review), these methods often lack the ability to learn to mimic the characteristics of a given dataset. This in turn limits the expressivity and fidelity of generated graphs and thus the range of possible applications of graph generative models.**

In this paper, we introduce a new model for generating GRAPhs via SPectral diffusion (**GGSD**). The ideas underpinning our approach are 1) to represent the graph using the eigendecomposition of its Laplacian matrix and 2) to use a diffusion-based approach to learn to sample sets of eigenvalues and eigenvectors from which a graph adjacency matrix can be reconstructed. Doing this allows us to work directly in the space of nodes while overcoming the computational bottleneck (quadratic in the number of graph nodes) of other methods that follow a similar approach Vignac et al. (2022). By limiting the number of eigenvalues and eigenvectors used to reconstruct the graph adjacency matrix, we reduce the complexity of the iterative denoising process to be linear with respect to the number

of nodes while, at the same time, having a representation tablet to encapsulate graph structural characteristics. Moreover, unlike other models conditioned on spectral representations Martinkus et al. (2022), our model also allows us to robustly condition the generation of new graphs on desired spectral properties (subsets of eigenvalues and/or eigenvectors) at inference time.

The remainder of this paper is structured as follows. Section 2 reviews the related work, while Sections 3 introduces the necessary background on denoising diffusion models. We introduce our graph generative model in Section 4, and we present the experimental evaluation against state-of-the-art alternatives in Section 5. Finally, Section 6 concludes the paper.

## 2 RELATED WORK

In contrast to the image and text domains, where the development of generative models is well understood and established, graphs introduce a series of additional challenges.

The first issue is the non-uniqueness of graph representations, *i.e.*, if a graph contains  $n$  nodes, there exist up to  $n!$  possibly distinct adjacency matrices that serve as equivalent representations of the same graph, since there is no reason to prefer a particular node order. Ideally, a generative model should assign equal probability to each of these  $n!$  adjacency matrices. Another crux lies in the size of the output space, which is quadratic in the number of nodes, and that quickly becomes a bottleneck when dealing with large graphs. Graph generative models should also be able to consider the existence of dependencies and relationships between nodes and edges, rather than treating them as independent, *e.g.*, in social networks the likelihood of two nodes being connected is often higher when they have common neighbors. Finally, standard machine learning techniques designed for continuously differentiable objective functions are unsuitable to be directly applied to discrete graph structures Guo & Zhao (2022).

**Seminal** graph generative model approaches seek to address these problems, yet focus only on the generation of graphs displaying a limited set of structural characteristics. These initial methods rely on identifying common characteristics in real-world graphs, such as degree distribution, graph diameter, and clustering coefficient Faloutsos (2008), and then generate synthetic graphs through the application of a set of heuristic rules Leskovec et al. (2010); Leskovec & Faloutsos (2007); Erdős et al. (1960); Albert & Barabási (2002). Although these models can produce synthetic graphs with the given desired features, they are limited in their ability to generate node features as well as novel structural patterns.

A breakthrough in this field has been marked by the recent progress in deep learning models such as Variational Auto Encoders (VAEs) Kingma & Welling (2013), Recurrent Neural Networks (RNNs) Zaremba et al. (2014) and Generative Adversarial Networks (GANs) Goodfellow et al. (2014). In this context, we encounter models commonly referred to as *general-purpose deep graph generative models*, such as GraphRNN You et al. (2018b) and GRAN Liao et al. (2019), which exploit deep architectures to learn the graphs distribution. Even though they represent a step forward in the field of generative graph models, most of them are limited by exclusively focusing on the graphs structure. Further, approaches of this type adopt evaluation metrics based only on graph statistics, like degree distribution or clustering coefficients, and thus overlook or omit the assessment of the generated node features.

Node and edge features are instead considered in a number of methods developed specifically for the generation of molecules, indeed one of the most promising application scenario for modern graph generation approaches. Models falling in this domain, referred to as *molecule graph generative models*, exploit deep architectures such as GAN in De Cao & Kipf (2018) or RNN in Popova et al. (2019) as well as other generation strategies (*e.g.*, graph normalizing flows Luo et al. (2021)) or the combination of different approaches. For instance, Shi et al. (2020) combines the advantages of both autoregressive and flow-based methods.

Nevertheless, there are other deep learning approaches beyond molecule graph generative models that are capable of generating graphs with node and edge features - even though the evaluation itself is often still based on a molecule generation task. For instance Simonovsky & Komodakis (2018) and Grover et al. (2019) propose general deep generative models for graphs based on variational autoencoders. The main drawback of these architectures is that they are specialized and limited to small-scale graphs with low-dimensional feature space Yoon et al. (2023).

Another category of graph generative models takes cues from the score-based generative modeling work of Song & Ermon (2019) to define diffusion models for graphs. For instance, in Huang et al. (2022) the authors propose a forward diffusion process, specifically a continuous-time generative diffusion process for permutation invariant graph generation. Similarly, Niu et al. (2020) introduce a different diffusion model named Edge-wise Dense Prediction Graph Neural Network (EDP-GNN), which uses Gaussian noise and uses thresholding to address the issue of generating a discrete valued adjacency matrix from continuous values. Crucially, the proposed method cannot fully capture node-edge dependencies. A similar score-based generative model for graphs, where both node features and adjacency matrix are created, is presented in Jo et al. (2022). Finally, Vignac et al. (2022) suggest an alternative approach where a discrete diffusion process is used to generate graphs with discrete node and edge features. This is similar to Haefeli et al. (2022), however the latter can only be applied to unattributed graphs.

More recently, Martinkus et al. (2022) with their SPECTRE network and Luo et al. (2023) take a different approach by considering the graph spectra, thus leveraging the inherent ability of the low frequency portion of the spectrum to capture global structural characteristics of the corresponding graph. **Although similar to our method, SPECTRE focuses on generating an adjacency matrix conditioned on a set of eigenvectors, which may or may not have been generated themselves. Our method instead only generates eigenpairs from which the adjacency matrix is recovered. As a result, unlike SPECTRE, our method is capable of generating graphs that respect a set of given spectral properties (see Subsection 5.4). GSDM Luo et al. (2023), on the other hand, proposes to reduce the complexity by performing diffusion just on the eigenvalues and optionally on the node features, while the eigenvectors used to reconstruct the final adjacency matrix are uniformly sampled from the training set.** DiGress Vignac et al. (2022) is also closely related to our model, however its complexity is quadratic in the number of nodes of the graph, making it unsuitable to work on large graphs.

**Our approach is also related to recently introduced latent graph diffusion models, which employ an autoencoder architecture to map nodes and edges of a graph to latent space where the diffusion process takes place Yang et al. (2024); Zhou et al. (2024). While these approaches aim to learn a low-dimensional embedding of the graph nodes, we rely instead on the well-established concept of spectral embedding Luo et al. (2003), with eigenvectors providing a low-dimensional embedding of the graph nodes and eigenvalues capturing global structure information.**

### 3 DENOISING DIFFUSION MODELS

Denosing Diffusion Probabilistic Models (DDPMs) are a class of generative models inspired by considerations from non-equilibrium thermodynamics. In particular, diffusion models in deep learning were first introduced in Sohl-Dickstein et al. (2015) yet popularized only in 2020 Ho et al. (2020). They operate by iteratively introducing noise to an input signal and then learning to denoise it thus generating new samples from the corrupted signals. Specifically, the idea is to destroy the structure in a data distribution through an iterative forward diffusion process (noising) and then learn a reverse diffusion process (denoising). This reverse process restores structure in the data, thus yielding a tractable generative model of the data.

Given a data point sampled from a real but unknown data distribution  $\mathbf{x}_0 \sim q(\mathbf{x})$ , we define a forward noising process  $q$  producing a sequence of noisy samples  $\mathbf{x}_1, \dots, \mathbf{x}_T$  as a Markov Chain given by  $q(\mathbf{x}_1, \dots, \mathbf{x}_T | \mathbf{x}_0) = \prod_{t=1}^T q(\mathbf{x}_t | \mathbf{x}_{t-1})$ , with the diffusion kernel defined as:

$$q(\mathbf{x}_t | \mathbf{x}_{t-1}) = \mathcal{N}\left(\mathbf{x}_t; \sqrt{1 - \beta_t} \mathbf{x}_{t-1}, \beta_t \mathbf{I}\right). \quad (1)$$

Note that, if we define  $\bar{\alpha}_t = \prod_{s=1}^t (1 - \beta_s)$ , we can reformulate Eq. 1 as a single step

$$q(\mathbf{x}_t | \mathbf{x}_0) = \mathcal{N}\left(\mathbf{x}_t; \sqrt{\bar{\alpha}_t} \mathbf{x}_0, (1 - \bar{\alpha}_t) \mathbf{I}\right). \quad (2)$$

In the reverse diffusion process, the goal is to recreate the true sample from a Gaussian noise input  $\mathbf{x}_T \sim \mathcal{N}(\mathbf{0}, \mathbf{I})$  by sampling from  $q(\mathbf{x}_{t-1} | \mathbf{x}_t)$ , the true denoising distribution. In order to run the reverse diffusion process, we need to learn a model  $p_\theta$ , often referred to as *score model*, to approximate these conditional probabilities. As Feller (1949) showed, in the case of Gaussian distributions the diffusion process reversal has the same functional form of the forward process. From this it

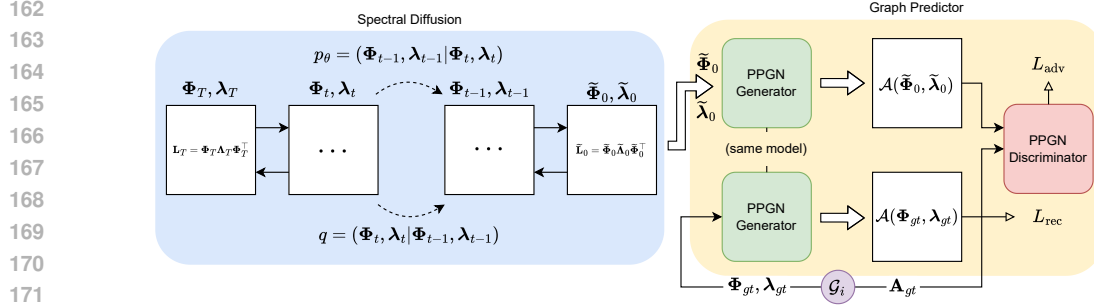


Figure 1: **GGSD** pipeline. During the spectral diffusion process (left) the neural network is trained to predict the denoising steps for the eigenvectors  $\phi$  and eigenvalues  $\lambda$  of the graph Laplacian. The second stage of our method is the graph predictor (right), where we train a Provably Powerful Graph Network (PPGN) Maron et al. (2019) (similar to what was done in SPECTRE Martinkus et al. (2022)). Given the eigenvalues and eigenvectors generated, it predicts the adjacency matrix.

follows that the reverse diffusion process kernel can be defined as

$$p_\theta(\mathbf{x}_{t-1} | \mathbf{x}_t) = \mathcal{N}(\mathbf{x}_{t-1}; \boldsymbol{\mu}_\theta(\mathbf{x}_t, t), \boldsymbol{\Sigma}_\theta(\mathbf{x}_t, t)), \quad (3)$$

where  $\theta$  are the parameters of the reverse diffusion kernel at each time step, which can be learned using a neural network. If we fix the variance to a constant  $\beta_t$  (*i.e.*  $\boldsymbol{\Sigma}_\theta(\mathbf{x}_t, t) = \beta_t I$ ), we only need to learn the distance between the means of two Gaussian distributions, *i.e.*, between the noise added in the forward process and the noise predicted by the model. This leads to a variational lower bound loss expressed in terms of the Kullback–Leibler (KL) divergence between the posterior of the forward process and the parameterized reverse diffusion process.

## 4 OUR METHOD

Consider an undirected unweighted graph  $\mathcal{G} = (\mathcal{V}, \mathcal{E})$ , where  $\mathcal{V}$  is the set of  $n$  nodes connected by the edge set  $\mathcal{E}$ . Recall that for a graph with adjacency matrix  $\mathbf{A}$ , the graph Laplacian  $\mathbf{L}$  is defined as  $\mathbf{L} = \mathbf{D} - \mathbf{A}$ , where  $\mathbf{D}$  is the diagonal degree matrix. Finally, let  $\Phi$  and  $\Lambda$  be the orthonormal matrix of eigenvectors (as columns) and the diagonal matrix of eigenvalues given by the eigendecomposition  $\mathbf{L} = \Phi \Lambda \Phi^\top$ , respectively. In the following sections, we use  $\lambda$  to denote the vector of eigenvalues of the graph Laplacian.

The fundamental intuition underpinning our model is that we can represent the graph connectivity with (possibly a subset of) the eigenvectors  $\Phi$  and the corresponding eigenvalues  $\lambda$  of the graph Laplacian. The connection between the spectrum of the graph Laplacian and the structural properties of the underlying graph is well known and studied. For example, it is well established that the low frequency portion of the spectrum captures the global structural characteristic of the graph, while the high frequencies are essential in the reconstruction of local connectivity patterns Chung (1997).

Fig. 1 shows an overview of the proposed pipeline. This is made of two main components, namely 1) a spectral diffusion process that generates a set of eigenvalues and eigenvectors from which an approximation of the Laplacian matrix can be reconstructed and 2) a graph predictor, which outputs a binary adjacency matrix from the (noisy) Laplacian reconstruction. The two components are discussed in detail in the following subsections.

### 4.1 SPECTRAL DIFFUSION

Moving from the Laplacian to its spectrum reduces the double row-, column-covariance with respect to node permutations of the Laplacian matrix, to a single covariance over the rows of the eigenvector matrix. To address this covariance, we represent the eigenvector matrix as a series of spectral embedding of the nodes, *i.e.*, we interpret the  $i$ -th component of the  $j$ -th eigenvector as the  $j$ -th component of the  $i$ -th node embedding, or alternatively, we see the rows of  $\Phi$  as vectors. To this we add the eigenvalues  $\lambda$  as a global graph descriptor. We can then define the **reverse** diffusion step as

$$p_\theta(\Phi_{t-1}, \lambda_{t-1} | \Phi_t, \lambda_t) = \mathcal{N}(\{\Phi_{t-1}, \lambda_{t-1}\}; \boldsymbol{\mu}_\theta(\Phi_t, \lambda_t, t), \sigma_t^2 \mathbf{I}) \quad (4)$$

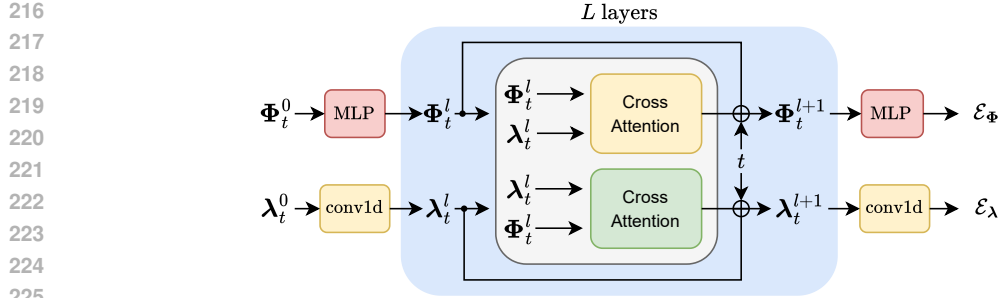


Figure 2: The score model takes as input the noisy eigenvector matrix and eigenvalues at time  $t$  and predicts the noise of the data to be used in the denoising step. The  $k$  node feature eigenvectors  $\Phi_t^0$  are projected through an MLP to a  $d$  dimensional space. The sequence of  $k$  eigenvalues is given as input to a 1D convolutional layer, which outputs  $d$  features for each eigenvalue. Both eigenvectors and eigenvalues go through a series of  $L$  layers composed of two multi-head cross-attention blocks, one updating the eigenvectors conditioned by the eigenvalues and one updating the eigenvalues conditioned on the eigenvectors. After each layer, we apply a residual block  $\oplus$ , which adds to the layer input the updated values scaled and shifted by time-dependent factors. Finally,  $\Phi_t^L$  and  $\lambda_t^L$  are projected to a  $k$  dimensional space through an MLP and a 1D convolution.

where the normal distribution is over the product set of the spectral embeddings and the global spectral descriptor.

Following DDPM Ho et al. (2020), we train a neural network to predict the denoising step. We design the backbone of our spectral diffusion process of Eq. 4 as a neural network composed of a sequence of layers containing a pair of multi-head attention blocks Vaswani et al. (2017), one operating on the eigenvectors conditioned on the eigenvalues and one operating on the eigenvalues conditioned by the eigenvectors. This choice allows us to achieve both a node permutation invariant model and to let the eigenvectors and eigenvalues condition each other on the prediction of the denoising step. Moreover, this model can easily handle node features  $\mathbf{X}$  by simply concatenating them to the eigenvectors of each node. Fig. 2 shows the overall structure of the proposed neural network. Note that the `conv1d` layer is applied to the eigenvalues, which are invariant with respect to node permutations, while the diffusion process itself acts in an invariant way on node embeddings, which are permutationally covariant. As a consequence, the whole process is permutationally invariant.

**Crucially, our model allows us to** reduce the memory footprint of the diffusion component from  $O(n^2)$  to  $O(kn)$ , where  $n$  denotes the number of graph nodes, by fixing the maximum number of eigenvectors to  $k$ , resulting in a faster generative process. For this reason, for larger graphs, we perform diffusion on a subset of  $k$  eigenvectors. In this case, after the denoising diffusion process, we obtain a subset  $\tilde{\Phi}$  of columns of  $\Phi$  with the corresponding subset of eigenvalues  $\tilde{\lambda}$ , which allows for an approximated reconstruction of  $\tilde{\mathbf{L}} = \tilde{\Phi}\tilde{\lambda}\tilde{\Phi} \approx \mathbf{L}$ , from which the adjacency matrix can be inferred. **In addition, since the eigenvector associated with the null eigenvalue does not contribute to the reconstruction of the Laplacian matrix, we can safely ignore it in the generation process.**

It should be noted that the optimal number of eigenvalues/eigenvectors ( $k$ ) to use is not fixed. We determined its range through preliminary analyses on the SBM and Planar datasets (see Appendix E), and in general, we treat it as a hyper-parameter of the model. Interestingly, our experiments reveal that the eigenvectors corresponding to the smallest eigenvalues (lowest frequencies) do not consistently offer more information about connectivity or result in better reconstructions of the original adjacency matrix.

## 4.2 GRAPH PREDICTOR

The main drawback of considering a subset of the eigenvectors is the introduction of noise on the reconstructed adjacency matrix. We adopt a strategy similar to the one proposed in SPECTRE Martinkus et al. (2022) to predict a binary adjacency matrix starting from a noisy reconstruction. We train a  $l$ -layer Provably Powerful Graph Network (PPGN) Maron et al. (2019), which takes as input the generated eigenvectors  $\tilde{\Phi}$  scaled by the square root of the eigenvalues  $\tilde{\lambda}$  as node features as well

Table 1: Comparison with other graph generative models using MMD metrics (the smaller, the better) on synthetic datasets.

	Community-Small				Planar				Stochastic Block Model (SBM)			
	Deg. ↓	Clus. ↓	Spect. ↓	Orb. ↓	Deg. ↓	Clus. ↓	Spect. ↓	Orb. ↓	Deg. ↓	Clus. ↓	Spect. ↓	Orb. ↓
GraphRNN	0.0271	0.1072	0.0520	0.1469	0.0096	0.2985	0.0389	1.4022	0.0178	0.0151	0.0104	0.0351
GRAN	<b>0.0013</b>	0.0843	0.0282	0.0201	0.0202	0.2985	0.0248	0.1964	0.0135	0.0149	<u>0.0034</u>	0.0352
DiGress	0.0096	0.1035	0.0506	0.0372	<b>0.0005</b>	<b>0.0178</b>	<b>0.0020</b>	0.0115	0.0166	0.0246	0.0064	0.1327
<b>GSDM</b>	0.0099	<b>0.0446</b>	<b>0.0131</b>	<u>0.0155</u>	0.0220	<u>0.0222</u>	0.0096	0.0371	0.2295	0.2280	0.1578	0.2876
GDSS	0.0107	0.1060	0.0450	0.0356	0.0701	<u>0.3025</u>	0.0403	1.0345	0.2658	0.0442	0.0551	0.2780
SPECTRE	0.0079	0.1067	0.0460	0.0250	0.0008	0.0859	0.0147	<u>0.0058</u>	<u>0.0044</u>	<u>0.0118</u>	<b>0.0015</b>	<b>0.0140</b>
<b>GGSD</b>	<u>0.0016</u>	<u>0.0590</u>	<u>0.0153</u>	<b>0.0142</b>	<u>0.0007</u>	0.1881	0.0125	<b>0.0047</b>	<b>0.0005</b>	<b>0.0115</b>	0.0045	<u>0.0289</u>

as the noisy adjacency matrix  $\tilde{\mathbf{A}} = \tilde{\mathbf{D}} - \tilde{\mathbf{L}}$  and predicts the binary adjacency matrix

$$\mathcal{A}(\tilde{\Phi}, \tilde{\lambda}) = \sigma(\text{PPGN}_l(\tilde{\mathbf{A}}, \tilde{\Phi} \tilde{\lambda}^{\frac{1}{2}})), \quad (5)$$

where  $\sigma$  is a sigmoid activation function and  $\text{PPGN}_l$  is a sequence of PPGN layers. We train this network with two losses: 1) a reconstruction loss on the eigenvectors  $\tilde{\Phi}_{gt}$  and eigenvalues  $\tilde{\lambda}_{gt}$  of the reduced spectrum of the training graphs with adjacency matrix  $\mathbf{A}_{gt}$  and 2) an adversarial loss on the generated adjacency matrix  $\mathcal{A}(\tilde{\Phi}, \tilde{\lambda})$ , *i.e.*,

$$L_{\text{rec}} = \text{BCE}(\mathbf{A}_{gt}, \mathcal{A}(\tilde{\Phi}_{gt}, \tilde{\lambda}_{gt})) \text{ and } L_{\text{adv}} = \log(\mathcal{D}(\mathbf{A}_{gt})) + \log(1 - \mathcal{D}(\mathcal{A}(\tilde{\Phi}, \tilde{\lambda}))), \quad (6)$$

where BCE is the standard binary cross entropy loss and  $\mathcal{D}$  is a discriminator network composed of a sequence of PPGN layers followed by a global pooling for the final graph-level classification. Note that, unlike in SPECTRE Martinkus et al. (2022), this refining step is not generative, meaning that the output is deterministic and depends solely on the input eigenvectors/values.

## 5 EXPERIMENTAL EVALUATION

**Datasets.** We compare the performance of our model against that of state-of-the-art alternatives on both synthetic and real-world datasets. As commonly done in the literature, we use three synthetic datasets and two real-world datasets. The synthetic datasets we consider are (i) Community-small ( $12 \leq |V| \leq 20$ ), (ii) Planar ( $|V| = 64$ ), and (iii) Stochastic Block Model (SBM) (2-5 communities and 20-40 nodes per community). The real-world datasets are both from the molecular domain, namely (i) Proteins (100-500 nodes) Dobson & Doig (2003) and (ii) QM9 (9 nodes) Ruddigkeit et al. (2012); Ramakrishnan et al. (2014). Detailed descriptions of all datasets can be found in Appendix A.

**Evaluation Metrics.** We assess the ability of the models to generate graphs with structural characteristics close to those of the training graphs by following the methodology outlined in Liao et al. (2019), which aims to address the difficulties of measuring likelihoods when evaluating autoregressive graph generative models reliant on orderings. In particular, we adopt the approach proposed by You et al. (2018b) and Li et al. (2018b) and used by many others Krawczuk et al. (2020) as well. Our evaluation centers on contrasting the distributions of graph statistics between the generated and actual graphs. Specifically, we consider the following key graph statistics: 1) degree distribution (Deg.), 2) clustering coefficient (Clus.), 3) eigenvalues of the normalized graph Laplacian (Spec.), and 4) the occurrence frequency of all 4-node orbits (Orb.). Moreover, for QM9, we follow the literature and evaluate the quality of the generated graphs by computing the validity of the generated molecules, their uniqueness, and their novelty w.r.t. to the molecules in the training set and viceversa Samanta et al. (2020); Guo & Zhao (2022). Detailed information on the evaluation metrics used can be found in Appendix B.

**Baselines.** We evaluate the effectiveness of our model by comparing it against a number of well-established graph generative models as well as some recently developed deep graph generative models. In particular, we consider GraphRNN You et al. (2018b), GRAN Liao et al. (2019), DiGress Vignac et al. (2022), SPECTRE Martinkus et al. (2022), GDSS Jo et al. (2022) and **GSDM** Luo et al. (2023). For the molecule generation task we also include GraphVAE Simonovsky & Komodakis (2018).

Table 2: Comparison on real datasets with other graph generative models. **Left:** on Proteins dataset using MMD metrics (the lower, the better) and mean  $\pm$  standard deviation (over 10 folds). **Right:** on QM9 molecules dataset based on (V)validity, (U)niqueness, and (N)ovelty metrics (the higher, the better). Method values denoted by \* are taken from Martinkus et al. (2022) while by  $\dagger$  from Vignac et al. (2022).

	Proteins				QM9			
	Deg. $\downarrow$	Clus. $\downarrow$	Spect $\downarrow$	Orbit $\downarrow$	Val. $\uparrow$	V.& U. $\uparrow$	V.& U.& N. $\uparrow$	
GraphRNN	0.0065 $\pm$ 0.0011	0.1658 $\pm$ 0.0088	0.0170 $\pm$ 0.0009	0.8142 $\pm$ 0.0273	GraphVAE*	0.5570	0.4200	0.2610
GRAN	0.0569 $\pm$ 0.0056	0.1622 $\pm$ 0.0092	0.0146 $\pm$ 0.0007	0.3430 $\pm$ 0.0363	DiGress $\dagger$	0.9900	0.9523	0.3180
<b>GGSD</b>	0.3792 $\pm$ 0.0041	0.4653 $\pm$ 0.0089	0.3024 $\pm$ 0.0032	0.9589 $\pm$ 0.0285	GDSS	0.8335	0.8281	<u>0.7257</u>
GDSS	0.0653 $\pm$ 0.0063	0.4160 $\pm$ 0.0089	0.0706 $\pm$ 0.0021	0.8168 $\pm$ 0.0118	SPECTRE*	0.8730	0.3120	0.2910
SPECTRE	0.0082 $\pm$ 0.0021	0.0988 $\pm$ 0.0071	0.0066 $\pm$ 0.0004	0.0328 $\pm$ 0.0039				
<b>GGSD</b>	<b>0.0014<math>\pm</math>0.0003</b>	<b>0.0856<math>\pm</math>0.0066</b>	<b>0.0059<math>\pm</math>0.0007</b>	<b>0.0296<math>\pm</math>0.0066</b>	<b>GGSD</b>	0.966	0.864	<b>0.847</b>

**Experimental Setup.** To maximize the robustness of the experimental results, we follow a slightly different experimental setup compared to previous works. Specifically, for the synthetic datasets, we decided to create a larger set of test graphs: 200 graphs for Planar and SBM, and 100 graphs for community-small. Accordingly, we let each model generate an equivalent number of graphs (200 for Planar and SBM, 100 for community-small) to compute the MMD measures. Due to the limited number of graphs in the Proteins dataset (see Appendix A), we also followed a different and more robust protocol to evaluate the generated graphs on this dataset. Rather than utilizing a single subset of the dataset as a test set, we created 10 folds (identical for each method) allowing us to report the average of each metric ( $\pm$  standard deviation) over the 10 folds. Further detailed information on the model settings and training setup, both for our model and the baselines, is provided in Appendix D.

## 5.1 EVALUATING THE GENERATED GRAPHS

**Synthetic Datasets** The experimental results for community-small, SBM, and Planar are shown in Table 1. In this table, we report the MMD metrics for the graph statistics, where the smaller the statistics, the better. The results of our method (**GGSD**) are chosen from those obtained using either the lower or upper range of eigenvalues. Specifically, for the Planar, the results refer to the 16 smallest eigenvalues, whereas for the community-small dataset and SBM we used the largest ones, 8 and 32 respectively. The best performance is highlighted in bold, while the second-best value is underlined. Overall, our model consistently achieves the best or second-best results across all datasets, with the exception of *Clus.* in Planar and *Spect.* in SBM and Planar. **We posit that the lower performance on planar graphs may be related to the behaviour of the eigenvectors of this type of graphs. Note in fact that there is no clear class structure in this dataset but rather the graphs are related by the (hard) property of planarity. Indeed, graphs with similar spectra can lie on opposite sides of the discrimination boundary, i.e., between planar and non-planar graphs. As such, the addition or removal of an edge connecting local substructures can easily break the planarity of the graph without significantly affecting its spectral representation.**

Finally, for Planar and SBM, we also evaluated the quality of the generated graphs in terms of validity, uniqueness, and novelty in Appendix C, showing the ability of our method to generate graphs that are at the same time valid, unique, and novel.

**Real-world Datasets** Results for real-world dataset generations on Proteins and QM9 are reported in Table 2, left and right, respectively. Also in this series of experiments, we achieve good performance. Again, we selected the best results from either the highest or lowest frequencies. Notably, for the Proteins dataset, we utilized the 16 smallest eigenvalues, while for QM9, we used the entire spectrum. The Proteins dataset is especially challenging due to the size of the graphs, which can reach 500 nodes. For this dataset, **GGSD** ranks as the best in all metrics Table 2 (left). QM9, on the other hand, is composed by small graphs of up to 9 nodes, with both node and edge features. In Table 2 (right), it is important to note that the last column is of particular interest as it summarizes all values, where we emerge as the second top performer.

## 5.2 GRAPH PREDICTOR ABLATION

Given that the “Graph Predictor” is trained using a discriminative loss, one may think that it is this component that is doing all the “heavy lifting” of the graph generation task, while the “Spectral Diffusion” may be just producing noisy data.

To assess that this is not the case, we designed an experiment training our model to predict all the eigenvectors and eigenvalues on the community-small dataset. The small size of the graphs in this datasets allows us to generate all the eigenvectors  $\Phi$  and eigenvalues  $\lambda$  and reconstruct the exact Laplacian  $L = \Phi \Lambda \Phi^T$  and the (almost) binary adjacency matrix  $A = D - L$ , where  $D$  is the diagonal of the Laplacian. To obtain a binary adjacency matrix, we further threshold  $A$  to get the actual edges of the generated graph (i.e., every entry above 0.5 is considered an edge).

In Table 3 we show three different configurations of our method: 1) “Only Diffusion”: we use the technique we just described, in which the graph is constructed directly from the generated  $\Phi$  and  $\lambda$  without using the “Graph Predictor”; 2) “Noise + Predictor”: we give as input to the “Graph Predictor” noise drawn from a Gaussian distribution; 3) “Diff. + Prediction”: this is the full model used in all the other experiments. For each configuration, we provide results for two cases: 1) using the full set of eigenpairs - all eigenbasis to train the model, and 2) using a subset of the eigenpairs - model trained using the 8 largest eigenvalues and their corresponding eigenvectors.

Reconstructing the graph directly from the Laplacian (referred to as “Only Diffusion”) using the complete spectrum yields the best results. Conversely, using either random noise or the reconstructed Laplacian as input to the Predictor results in significantly inferior outcomes. This suggests that the “Spectral Diffusion” part of the network is responsible for the actual generation process. On the other hand, if we consider a truncated eigenbase for the training phase, the Predictor becomes useful as it helps to refine the results further.

To provide a comprehensive overview, we also provide some qualitative examples in Figure 3, comparing the eigenvectors generated by the diffusion module of **GGSD** with those of the Laplacian computed on the adjacency matrix predicted by the PPGN module. In smaller graphs, the eigenvectors are almost perfectly preserved, while only minor local differences emerge in larger graphs. In contrast, the generative approach used by SPECTRE fails to maintain the relationship between the conditioning eigenvectors and the final generated graph.

## 5.3 EIGENVECTORS ORTHOGONALITY

The general framework of DDPM cannot guarantee the orthonormality of the generated eigenvectors. While in principle this might pose a problem, in practice we observed that this property is well preserved in the generations. In Appendix F, we present both quantitative and qualitative analyses to evaluate the orthogonality of the generated eigenvectors, demonstrating that they exhibit approximate orthonormality. Moreover, in order to test if having an exact orthonormality of the eigenvectors brings any advantage, we tried to reproject the final generated eigenvectors to an orthonormal matrix through QR decomposition before the PPGN predictor step. As reported in Figure 4, we did not observe a clear benefit in having orthonormal basis. We argue that, even if orthonormality is a well-known characteristic of the eigendecomposition of the graph Laplacian (indeed, of the eigendecomposition of **any symmetric** matrix), it is probably not the most important (nor essential) to guarantee a good reconstruction of a valid graph Laplacian, which exhibits more complex properties that need to be learned directly from data.

Table 3: Ablation of the Graph Predictor network on the community-small dataset.

	Full Set of Eigenpairs				First 8 Eigenpairs			
	Deg. ↓	Clus. ↓	Spect. ↓	Orb. ↓	Deg. ↓	Clus. ↓	Spect. ↓	Orb. ↓
Only Diffusion	<b>0.00134</b>	<b>0.05484</b>	<b>0.01574</b>	<b>0.00514</b>	0.00936	0.09753	0.04341	0.01255
Noise + Predictor	0.04428	0.11129	0.05691	0.46051	0.06681	0.12330	0.05972	0.45137
Diff. + Predictor	0.00562	0.07887	0.02232	0.00942	<b>0.00423</b>	<b>0.05464</b>	<b>0.01832</b>	<b>0.00866</b>



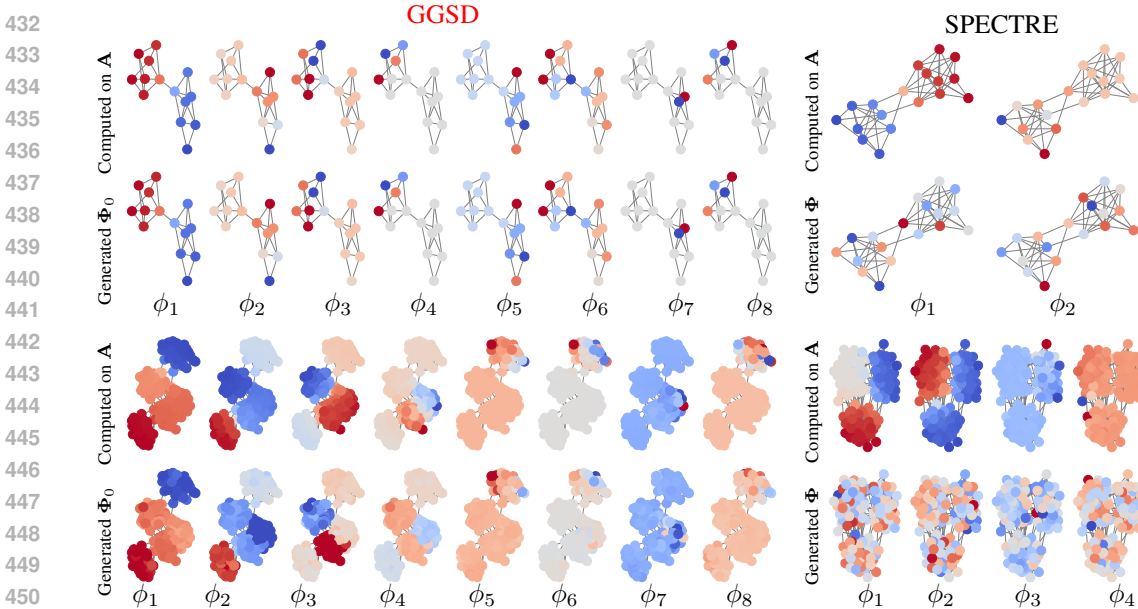


Figure 3: **Left column:** Comparison of the eigenvectors generated by the diffusion module of GGSD with the eigenvectors recomputed on the Laplacian computed on the adjacency matrix predicted by the PPGN module on the Community (top) and SBM (bottom) datasets. The models have been trained with the 8 smallest eigenvectors. In the smaller dataset (Community) the diffusion generates nearly perfect eigenvectors. In the more challenging SBM dataset we can notice that the generated eigenfunction are slightly different from the one computed on the predicted graph while preserving the overall structure. **Right column:** comparison of the interpolated eigenvectors that SPECTRE uses to condition the PPGN module to the actual eigenvectors of the generated graph. In this case the eigenvectors structure is completely lost in the generative process.

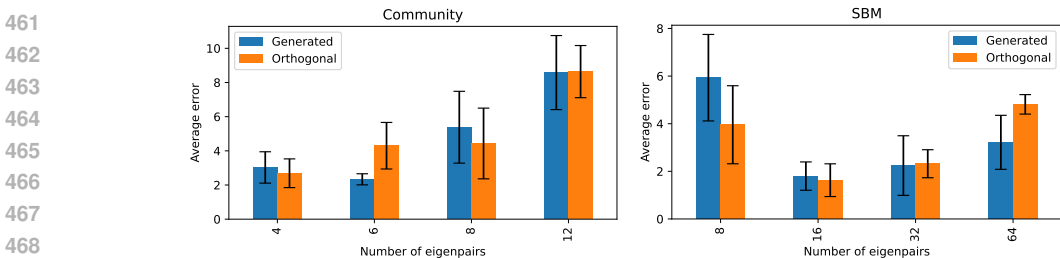


Figure 4: Performance analysis without (Generated) and with (Orthonormal) reprojecting the generated eigenvectors to an orthonormal basis. The average error represents the mean degradation of metrics between the generated graphs and the training set. We report both the mean and the standard deviation as error bars on 10 generations of 200 graphs. Specifically, Degree, Cluster, and Spectral metrics are calculated between the generated graphs and the test set, then normalized by the metrics between the training and test sets.

#### 5.4 SPECTRAL CONDITIONED GENERATION

The spectrum of the Laplacian plays a relevant role in many applications, ranging from graph classification and mesh analysis Bai et al. (2015); Hu et al. (2014) to reconstructing the underlying geometry of a triangulated 3D shape Cosmo et al. (2019); Marin et al. (2021). Being able to generate a graph given a target spectrum is thus an important feature of a generative method. We pose the graph generation conditioned on a sequence of eigenvalues and/or eigenvectors as an inpainting problem Lugmayr et al. (2022).

**Eigenvalues conditioned generation** In this setup, the eigenvectors at time  $t - 1$  are computed according to Eq. 4, while the eigenvalues are derived from the target ones through the diffusion

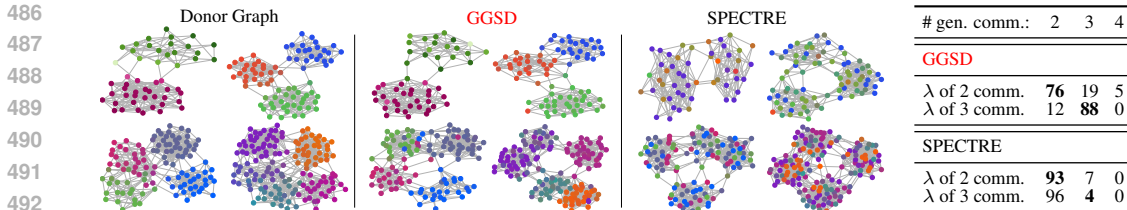


Figure 5 & Table 4: Conditioning of the generation on the first 3 smallest eigenvectors as an inpainting task using RePaint Lugmayr et al. (2022) (Figure). Number of communities in the graphs generated with spectrum conditioning (Table). Higher values should appear in the bold diagonal.

process (Eq. 2):

$$\lambda_{t-1} \sim \mathcal{N}(\sqrt{\bar{\alpha}_t} \lambda_0, (1 - \bar{\alpha}_t) \mathbf{I}), \quad \Phi_{t-1} \sim \mathcal{N}(\Phi_{t-1}; \mu_\theta(\Phi_t, \lambda_t; t), \beta_t \mathbf{I}). \quad (7)$$

To validate the generation conditioned on the eigenvalues, we generate graphs of the SBM data distribution by fixing the number of nodes as the average number of nodes of graphs containing 2 and 3 communities (70 nodes). We randomly choose one graph with 2 communities and one graph with 3 communities from the test set, and we consider their spectra. We use these to condition the generation of two sets of 100 graphs, for the 2 and 3 communities eigenvalue sequences, respectively. The results reported in Table 4 show that spectral conditioning is able to influence the properties of the generated graphs, while the spectral conditioning provided by SPECTRE fails to preserve this property.

**Eigenvectors conditioned generation** We adopt a similar strategy for conditioning on a subset of the eigenvectors. In this case, just the portion of  $k'$  known eigenvectors  $\Phi' = [\phi_0, \dots, \phi_{k'}]$  at time  $t - 1$  is computed according to Eq. 4, while the remaining eigenvectors  $\bar{\Phi}' = [\phi_{k'+1}, \dots, \phi_k]$  and the eigenvalues are derived from the target ones through the forward diffusion process. The three groups of 4 graphs in Figure 5 show the donor graphs (left) from which the first three eigenvectors were computed, the graphs conditioned on the given eigenvectors using GGSD (center) and SPECTRE (right). The color is the 2D color encoding of 2 of the three first eigenvectors manually selected to highlight the different clusters. The colors from the donor graph have then been transported on the generated graphs' corresponding node (same node index). While GGSD is able to preserve the community structure encoded by the given eigenvectors, in SPECTRE, this information is completely lost, causing nodes from the same community in the donor graph to randomly spread over different communities of the generated graph. This in turn may be due to the particular generation mechanism of SPECTRE. Specifically, SPECTRE learns a set of reduced orthogonal bases during training, which are left and right-rotated according to a rotation matrix predicted by a PointNetST Segol & Lipman (2019) network based on some input (generated) eigenvalues. This requires an alignment of the graphs to the learned bases, which makes the training more complex. Our approach, on the other hand, is fully covariant.

## 6 CONCLUSION

We have introduced GGSD, a diffusion-based generative model for graphs where the spectrum of the graph Laplacian is used to retain structural information while reducing the computational complexity. Our approach has a number of advantages, from the ability to directly generate eigenvectors and eigenvalues, to the possibility of naturally encapsulate node feature information as well as conditioning the generation on target spectral properties.

Our model suffers from two main limitations. Firstly, while using low/high frequencies to reconstruct the spectrum is theoretically grounded, in practice it would be interesting to allow the model to select the most informative frequencies for a given dataset. We will explore this possibility in future work. Secondly, while the diffusion model is linear, the bottleneck of our model is the PPGN-based predictor, which has quadratic complexity. In the future, it would be interesting to investigate alternative methods employing a sparse representation of the adjacency matrix reconstructed from the Laplacian.

## REFERENCES

- 540  
541  
542 Réka Albert and Albert-László Barabási. Statistical mechanics of complex networks. *Reviews of*  
543 *modern physics*, 74(1):47, 2002.
- 544 Lu Bai, Luca Rossi, Andrea Torsello, and Edwin R Hancock. A quantum jensen–shannon graph  
545 kernel for unattributed graphs. *Pattern Recognition*, 48(2):344–355, 2015.
- 546  
547 Fan RK Chung. *Spectral graph theory*, volume 92. American Mathematical Soc., 1997.
- 548 Luca Cosmo, Mikhail Panine, Arianna Rampini, Maks Ovsjanikov, Michael M. Bronstein, and  
549 Emanuele Rodolà. Isospectralization, or how to hear shape, style, and correspondence. In  
550 *IEEE Conference on Computer Vision and Pattern Recognition, CVPR 2019, Long Beach, CA,*  
551 *USA, June 16-20, 2019*, pp. 7529–7538. Computer Vision Foundation / IEEE, 2019. doi:  
552 10.1109/CVPR.2019.00771.
- 553 Nicola De Cao and Thomas Kipf. Molgan: An implicit generative model for small molecular graphs.  
554 *arXiv preprint arXiv:1805.11973*, 2018.
- 555  
556 Hubert de Fraysseix and Patrice Ossona de Mendez. Trémaux trees and planarity. *European Jour-*  
557 *nal of Combinatorics*, 33(3):279–293, 2012. ISSN 0195-6698. doi: [https://doi.org/10.1016/j.ejc.](https://doi.org/10.1016/j.ejc.2011.09.012)  
558 2011.09.012. URL [https://www.sciencedirect.com/science/article/pii/](https://www.sciencedirect.com/science/article/pii/S0195669811001600)  
559 [S0195669811001600](https://www.sciencedirect.com/science/article/pii/S0195669811001600). Topological and Geometric Graph Theory.
- 560 Paul D Dobson and Andrew J Doig. Distinguishing enzyme structures from non-enzymes without  
561 alignments. *Journal of molecular biology*, 330(4):771–783, 2003.
- 562 Mikhail Drobyshvskiy and Denis Turdakov. Random graph modeling: A survey of the concepts.  
563 *ACM computing surveys (CSUR)*, 52(6):1–36, 2019.
- 564 Paul Erdős, Alfréd Rényi, et al. On the evolution of random graphs. *Publ. math. inst. hung. acad.*  
565 *sci*, 5(1):17–60, 1960.
- 566  
567 Ludwig Fahrmeir, Thomas Kneib, Stefan Lang, Brian Marx, Ludwig Fahrmeir, Thomas Kneib,  
568 Stefan Lang, and Brian Marx. *Regression models*. Springer, 2013.
- 569  
570 Christos Faloutsos. Graph mining: Laws, generators and tools. *Lecture Notes in Computer Science*,  
571 5012:1, 2008.
- 572 W. Feller. On the theory of stochastic processes, with particular reference to applications. In *Pro-*  
573 *ceedings of the [First] Berkeley Symposium on Mathematical Statistics and Probability*, pp. 403–  
574 432, 1949.
- 575  
576 Rafael Gómez-Bombarelli, Jennifer N Wei, David Duvenaud, José Miguel Hernández-Lobato,  
577 Benjamín Sánchez-Lengeling, Dennis Sheberla, Jorge Aguilera-Iparraguirre, Timothy D Hirzel,  
578 Ryan P Adams, and Alán Aspuru-Guzik. Automatic chemical design using a data-driven contin-  
579 uous representation of molecules. *ACS central science*, 4(2):268–276, 2018.
- 580 Ian Goodfellow, Jean Pouget-Abadie, Mehdi Mirza, Bing Xu, David Warde-Farley, Sherjil Ozair,  
581 Aaron Courville, and Yoshua Bengio. Generative adversarial nets. *Advances in neural information*  
582 *processing systems*, 27, 2014.
- 583 Aditya Grover, Aaron Zweig, and Stefano Ermon. Graphite: Iterative generative modeling of graphs.  
584 In *International conference on machine learning*, pp. 2434–2444. PMLR, 2019.
- 585  
586 Xiaojie Guo and Liang Zhao. A systematic survey on deep generative models for graph generation.  
587 *IEEE Transactions on Pattern Analysis and Machine Intelligence*, 45(5):5370–5390, 2022.
- 588  
589 Kilian Konstantin Haefeli, Karolis Martinkus, Nathanaël Perraudin, and Roger Wattenhofer. Dif-  
590 fusion models for graphs benefit from discrete state spaces. *arXiv preprint arXiv:2210.01549*,  
591 2022.
- 592  
593 Jonathan Ho, Ajay Jain, and Pieter Abbeel. Denoising diffusion probabilistic models. *Advances in*  
*neural information processing systems*, 33:6840–6851, 2020.

- 594 Nan Hu, Raif M Rustamov, and Leonidas Guibas. Stable and informative spectral signatures for  
595 graph matching. In *Proceedings of the IEEE conference on computer vision and pattern recogni-*  
596 *tion*, pp. 2305–2312, 2014.
- 597 Han Huang, Leilei Sun, Bowen Du, Yanjie Fu, and Weifeng Lv. Graphgdp: Generative diffusion  
598 processes for permutation invariant graph generation. In *2022 IEEE International Conference on*  
599 *Data Mining (ICDM)*, pp. 201–210. IEEE, 2022.
- 600 Jaehyeong Jo, Seul Lee, and Sung Ju Hwang. Score-based generative modeling of graphs via the  
601 system of stochastic differential equations. In *International Conference on Machine Learning*,  
602 pp. 10362–10383. PMLR, 2022.
- 603 Diederik P Kingma and Max Welling. Auto-encoding variational bayes. *arXiv preprint*  
604 *arXiv:1312.6114*, 2013.
- 605 Igor Krawczuk, Pedro Abranches, Andreas Loukas, and Volkan Cevher. Gg-gan: A geometric graph  
606 generative adversarial network. 2020.
- 607 Jure Leskovec and Christos Faloutsos. Scalable modeling of real graphs using kronecker multipli-  
608 cation. In *Proceedings of the 24th international conference on Machine learning*, pp. 497–504,  
609 2007.
- 610 Jure Leskovec, Deepayan Chakrabarti, Jon Kleinberg, Christos Faloutsos, and Zoubin Ghahramani.  
611 Kronecker graphs: an approach to modeling networks. *Journal of Machine Learning Research*,  
612 11(2), 2010.
- 613 Yibo Li, Liangren Zhang, and Zhenming Liu. Multi-objective de novo drug design with conditional  
614 graph generative model. *Journal of cheminformatics*, 10:1–24, 2018a.
- 615 Yujia Li, Oriol Vinyals, Chris Dyer, Razvan Pascanu, and Peter Battaglia. Learning deep generative  
616 models of graphs. *arXiv preprint arXiv:1803.03324*, 2018b.
- 617 Renjie Liao, Yujia Li, Yang Song, Shenlong Wang, Will Hamilton, David K Duvenaud, Raquel  
618 Urtasun, and Richard Zemel. Efficient graph generation with graph recurrent attention networks.  
619 *Advances in neural information processing systems*, 32, 2019.
- 620 Andreas Lugmayr, Martin Danelljan, Andres Romero, Fisher Yu, Radu Timofte, and Luc Van Gool.  
621 Repaint: Inpainting using denoising diffusion probabilistic models. 2022.
- 622 Bin Luo, Richard C Wilson, and Edwin R Hancock. Spectral embedding of graphs. *Pattern recog-*  
623 *nition*, 36(10):2213–2230, 2003.
- 624 Tianze Luo, Zhanfeng Mo, and Sinno Jialin Pan. Fast graph generation via spectral diffusion. *IEEE*  
625 *Transactions on Pattern Analysis and Machine Intelligence*, 2023.
- 626 Youzhi Luo, Keqiang Yan, and Shuiwang Ji. Graphdf: A discrete flow model for molecular graph  
627 generation. In *International Conference on Machine Learning*, pp. 7192–7203. PMLR, 2021.
- 628 Riccardo Marin, Arianna Rampini, Umberto Castellani, Emanuele Rodolà, Maks Ovsjanikov, and  
629 Simone Melzi. Spectral shape recovery and analysis via data-driven connections. *Int. J. Comput.*  
630 *Vision*, 129(10):2745–2760, oct 2021. ISSN 0920-5691. doi: 10.1007/s11263-021-01492-6.
- 631 Haggai Maron, Heli Ben-Hamu, Hadar Serviansky, and Yaron Lipman. Provably powerful  
632 graph networks. In H. Wallach, H. Larochelle, A. Beygelzimer, F. d'Alché-Buc, E. Fox, and  
633 R. Garnett (eds.), *Advances in Neural Information Processing Systems*, volume 32. Curran  
634 Associates, Inc., 2019. URL [https://proceedings.neurips.cc/paper\\_files/](https://proceedings.neurips.cc/paper_files/paper/2019/file/bb04af0f7ecaee4aae62035497da1387-Paper.pdf)  
635 [paper/2019/file/bb04af0f7ecaee4aae62035497da1387-Paper.pdf](https://proceedings.neurips.cc/paper_files/paper/2019/file/bb04af0f7ecaee4aae62035497da1387-Paper.pdf).
- 636 Karolis Martinkus, Andreas Loukas, Nathanaël Perraudin, and Roger Wattenhofer. Spectre: Spectral  
637 conditioning helps to overcome the expressivity limits of one-shot graph generators. In *Internat-*  
638 *ional Conference on Machine Learning*, pp. 15159–15179. PMLR, 2022.
- 639 Chenhao Niu, Yang Song, Jiaming Song, Shengjia Zhao, Aditya Grover, and Stefano Ermon. Per-  
640 mutation invariant graph generation via score-based generative modeling. In *International Con-*  
641 *ference on Artificial Intelligence and Statistics*, pp. 4474–4484. PMLR, 2020.

- 648 Tiago P. Peixoto. Hierarchical block structures and high-resolution model selection in large net-  
649 works. *Phys. Rev. X*, 4:011047, Mar 2014. doi: 10.1103/PhysRevX.4.011047. URL <https://link.aps.org/doi/10.1103/PhysRevX.4.011047>.  
650  
651
- 652 Mariya Popova, Mykhailo Shvets, Junier Oliva, and Olexandr Isayev. Molecularrnn: Generating  
653 realistic molecular graphs with optimized properties. *arXiv preprint arXiv:1905.13372*, 2019.  
654
- 655 Raghunathan Ramakrishnan, Pavlo O Dral, Matthias Rupp, and O Anatole Von Lilienfeld. Quantum  
656 chemistry structures and properties of 134 kilo molecules. *Scientific data*, 1(1):1–7, 2014.  
657
- 658 Emanuele Rodolà, Luca Cosmo, Michael M Bronstein, Andrea Torsello, and Daniel Cremers. Partial  
659 functional correspondence. In *Computer graphics forum*, volume 36, pp. 222–236. Wiley Online  
660 Library, 2017.
- 661 Lars Ruddigkeit, Ruud Van Deursen, Lorenz C Blum, and Jean-Louis Reymond. Enumeration of 166  
662 billion organic small molecules in the chemical universe database gdb-17. *Journal of chemical  
663 information and modeling*, 52(11):2864–2875, 2012.
- 664 Bidisha Samanta, Abir De, Gourhari Jana, Vicenç Gómez, Pratim Chattaraj, Niloy Ganguly, and  
665 Manuel Gomez-Rodriguez. Nevae: A deep generative model for molecular graphs. *Journal of  
666 machine learning research*, 21(114):1–33, 2020.  
667
- 668 Nimrod Segol and Yaron Lipman. On universal equivariant set networks. In *International Confer-  
669 ence on Learning Representations*, 2019.
- 670 Chence Shi, Minkai Xu, Zhaocheng Zhu, Weinan Zhang, Ming Zhang, and Jian Tang.  
671 Graphaf: a flow-based autoregressive model for molecular graph generation. *arXiv preprint  
672 arXiv:2001.09382*, 2020.  
673
- 674 Martin Simonovsky and Nikos Komodakis. Graphvae: Towards generation of small graphs using  
675 variational autoencoders. In *Artificial Neural Networks and Machine Learning–ICANN 2018:  
676 27th International Conference on Artificial Neural Networks, Rhodes, Greece, October 4-7, 2018,  
677 Proceedings, Part I 27*, pp. 412–422. Springer, 2018.
- 678 Jascha Sohl-Dickstein, Eric Weiss, Niru Maheswaranathan, and Surya Ganguli. Deep unsupervised  
679 learning using nonequilibrium thermodynamics. In *International conference on machine learn-  
680 ing*, pp. 2256–2265. PMLR, 2015.  
681
- 682 Yang Song and Stefano Ermon. Generative modeling by estimating gradients of the data distribution.  
683 *Advances in neural information processing systems*, 32, 2019.  
684
- 685 Ashish Vaswani, Noam Shazeer, Niki Parmar, Jakob Uszkoreit, Llion Jones, Aidan N Gomez,  
686 Łukasz Kaiser, and Illia Polosukhin. Attention is all you need. In I. Guyon, U. Von  
687 Luxburg, S. Bengio, H. Wallach, R. Fergus, S. Vishwanathan, and R. Garnett (eds.), *Ad-  
688 vances in Neural Information Processing Systems*, volume 30. Curran Associates, Inc.,  
689 2017. URL [https://proceedings.neurips.cc/paper\\_files/paper/2017/  
690 file/3f5ee243547dee91fbd053c1c4a845aa-Paper.pdf](https://proceedings.neurips.cc/paper_files/paper/2017/file/3f5ee243547dee91fbd053c1c4a845aa-Paper.pdf).
- 691 Clement Vignac, Igor Krawczuk, Antoine Siraudin, Bohan Wang, Volkan Cevher, and Pas-  
692 cal Frossard. Digress: Discrete denoising diffusion for graph generation. *arXiv preprint  
693 arXiv:2209.14734*, 2022.
- 694
- 695 Duncan J Watts and Steven H Strogatz. Collective dynamics of ‘small-world’ networks. *nature*, 393  
696 (6684):440–442, 1998.
- 697 Ling Yang, Zhilin Huang, Zhilong Zhang, Zhongyi Liu, Shenda Hong, Wentao Zhang, Wenming  
698 Yang, Bin Cui, and Luxia Zhang. Graphusion: Latent diffusion for graph generation. *IEEE  
699 Transactions on Knowledge and Data Engineering*, 2024.
- 700
- 701 Minji Yoon, Yue Wu, John Palowitch, Bryan Perozzi, and Russ Salakhutdinov. Graph generative  
model for benchmarking graph neural networks. 2023.

702 Jiaxuan You, Bowen Liu, Zhitao Ying, Vijay Pande, and Jure Leskovec. Graph convolutional policy  
703 network for goal-directed molecular graph generation. *Advances in neural information processing*  
704 *systems*, 31, 2018a.

705  
706 Jiaxuan You, Rex Ying, Xiang Ren, William Hamilton, and Jure Leskovec. Graphrnn: Generat-  
707 ing realistic graphs with deep auto-regressive models. In *International conference on machine*  
708 *learning*, pp. 5708–5717. PMLR, 2018b.

709 Wojciech Zaremba, Ilya Sutskever, and Oriol Vinyals. Recurrent neural network regularization.  
710 *arXiv preprint arXiv:1409.2329*, 2014.

711  
712 Cai Zhou, Xiyuan Wang, and Muhan Zhang. Unifying generation and prediction on graphs with  
713 latent graph diffusion. In *The Thirty-eighth Annual Conference on Neural Information Processing*  
714 *Systems*, 2024.

715  
716  
717  
718  
719  
720  
721  
722  
723  
724  
725  
726  
727  
728  
729  
730  
731  
732  
733  
734  
735  
736  
737  
738  
739  
740  
741  
742  
743  
744  
745  
746  
747  
748  
749  
750  
751  
752  
753  
754  
755

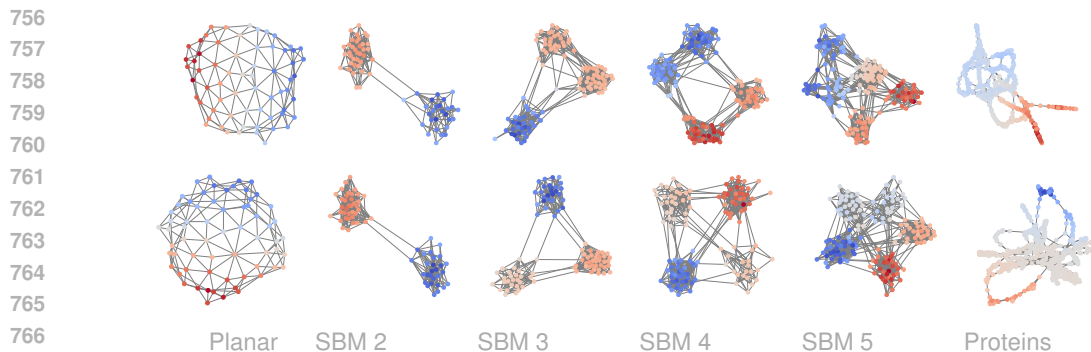


Figure 6: Visual comparison between training set graph samples and generated graph samples produced by **GGSD**. Each column represents a graph type (Planar, Stochastic Block Model with 2,3,4, and 5 communities, and Proteins). Top row (Original): training set graphs. Bottom row (Generated): graph generated by **GGSD**.

## A DATASETS.

We utilize five commonly used datasets for graph generative tasks. Some examples of the graphs contained in these datasets alongside a similar graph generated by **GGSD** are shown in Figure 6.

**Community-small**: A synthetic dataset consisting of 100 random community graphs, with  $[12, 20]$  nodes.

**Stochastic Block Model (SBM)**: A synthetic dataset from Martinkus et al. (2022) comprising 200 Stochastic Block Model graphs, each with a random selection of 2 to 5 communities and 20 to 40 nodes within each community. The probability of edges between communities is set at 0.3, while the probability of edges within communities is set at 0.05.

**Planar**: A synthetic dataset from Martinkus et al. (2022) of 200 planar graphs, each containing 64 nodes. Graphs are created through the application of Delaunay triangulation to a randomly and uniformly placed set of points.

**QM9** Ramakrishnan et al. (2014); Ruddigkeit et al. (2012): This real-world dataset comprises 134k organic molecules with a maximum of 9 heavy atoms (carbon, oxygen, nitrogen, and fluorine). By following Simonovsky & Komodakis (2018) we allocate 10k molecules for validation, 10k for testing, and the rest for training.

**Proteins** Dobson & Doig (2003): The dataset encompasses 918 protein graphs, each ranging from 100 to 500 nodes. In this representation, each protein is depicted as a graph, with nodes corresponding to amino acids. Nodes are connected by an edge if they are within a distance of less than 6 Angstroms from each other.

## B EVALUATION METRICS

### B.1 STATISTICS-BASED

We consider the following key graph statistics: degree distribution (Deg.), clustering coefficient (Clus.), and the occurrence frequency of all 4-node orbits (Orb.). The deviation of these metrics between the generated graphs and the actual ones is measured using the maximum mean discrepancy (MMD) You et al. (2018b). In its initial formulation, the computation of the MMD relied on the Earth Mover’s Distance (EMD) and as a result was very slow. For this reason, as suggested in Liao et al. (2019), we use the total variational (TV) Gaussian kernel. This in turn significantly accelerates the evaluation process while maintaining consistency with EMD. In addition to assessing node degree, clustering coefficient, and orbit counts, we also extend our evaluation to include a spectral analysis (Spect.), following Liao et al. (2019). This involves computing the eigenvalues of the normalized graph Laplacian, quantized to approximate a probability density. The spectral

Table 5: Comparison with other graph generative models based on validity, uniqueness, and novelty metrics (the higher the better) on synthetic datasets.

	Planar				Stochastic Block Model (SBM)			
	Val.↑	Uniq.↑	Nov.↑	V&U&N↑	Val.↑	Uniq.↑	Nov.↑	V&U&N↑
GraphRNN	0.00	-	-	0.00	0.13	1.00	1.00	0.13
GRAN	0.03	1.00	1.00	0.03	0.20	1.00	1.00	0.20
DiGress	0.70	0.98	0.95	<b>0.65</b>	0.13	0.98	1.00	0.13
GSDM	0.85	0.50	0.28	0.12	0.08	0.88	0.50	0.04
GDSS	0.00	-	-	0.00	0.01	1.00	1.00	0.01
SPECTRE	0.14	1.00	1.00	0.14	0.51	1.00	1.00	<b>0.51</b>
<b>GGSD</b>	0.15	1.00	1.00	<u>0.15</u>	0.49	1.00	1.00	<u>0.49</u>

comparison offers insights into the global properties of the graphs, complementing the local graph statistics emphasized by previous metrics.

## B.2 INTRINSIC-QUALITY-BASED

The *validity* is determined by the ratio of valid molecules to all generated molecules. For molecule graphs (QM9), the validity in molecule generation represents the percentage of chemically valid molecules based on specific domain rules. We measure it using RDKit antization<sup>1</sup>. For Planar graphs, we use the NetworkX python library based on the left-right planarity test (de Fraysseix & Ossona de Mendez, 2012). For the stochastic block model graphs (SBM), we use a Monte Carlo and greedy heuristic for the inference of the stochastic block model parameters (as implemented by cdlib (Peixoto, 2014)). We consider a graph valid if its probability, assessed by a Wald test (Fahrmeir et al., 2013), of having been generated by the SBM model with inter-edge probability of 0.3 and intra-edge probability of 0.005 is higher than 0.9, and if the number of communities is in the range 2-5 with a number of nodes for each community between 20 and 40.

The *novelty* gauges the percentage of **valid** graphs that are not sub-graphs of the training set, and vice versa. It checks if the model has successfully learned to generalize to unseen graphs and it considers two graphs identical if they are isomorphic.

The *uniqueness* is defined as the ratio of unique samples to valid **and novel** samples, measuring the level of variety during sampling. To calculate uniqueness, generated graphs that are sub-graph isomorphic to others are initially removed, and the remaining percentage represents uniqueness. For instance, if a model generates 100 identical graphs, the uniqueness is  $1/100 = 1\%$ .

The product of these three metrics is referred to as V&U&N (or VUN) and summarizes the ability of the method to generate graphs that are at the same time novel, unique, and valid.

## C VUN EXPERIMENTS

Table 5 presents the results on the quality of the synthetic graphs generated for the Planar and SBM datasets, analyzing the metrics of validity, uniqueness, novelty, and their combination. As highlighted in Section 5.1, our method achieves 100% uniqueness and novelty on both datasets while showing the second-best score in terms of VUN. Specifically, for SBM, the gap of SPECTRE and our method with respect to other methods is considerable, due to a higher validity score compared to competitors. On the other hand, the validity score of our method on the Planar dataset is lower than the top-performing method (DiGress) of some margin. This behavior is not unexpected and can be explained by the insensibility of the eigenvectors to small local changes of the topology as discussed in Section 5.1. It is worth noticing how GSDM, despite showing the best validity performance on planar graphs, is not able to generate novel graphs, with a novelty score of just 28% in Planar, and 50% in SBM. This does not come as a surprise, since in GSDM the eigenvectors used to reconstruct the final adjacency matrix are uniformly sampled from the training set. This limits the generative power of the method, since most of the information about the graph connectivity is contained in the

<sup>1</sup>[https://www.rdkit.org/docs/RDKit\\_Book.html](https://www.rdkit.org/docs/RDKit_Book.html)



eigenvectors. As such, the obtained graphs are not actually generated but rather slight modifications of the training set graphs.

## D MODEL SETTINGS AND IMPLEMENTATION DETAILS

For all datasets except for QM9, we retrained the models using the configurations recommended by the authors. When no recommended hyper-parameters setups or model weights were available, we explored the space of hyper-parameters tuning them according to the ranges mentioned for other datasets. Finally, for our method (GGSD), we use the  $k$  largest/smallest eigenvalues of the unnormalized Laplacian. The values of  $k$  are experimentally determined as explained in Appendix E. We stress that these are only a fraction of the full set of eigenvectors.

We used the unnormalized Laplacian since it yields an easier graph reconstruction by simple thresholding (as explained in Section 5.2). In order to handle potential scaling issues, we simply normalized the eigenvalues and eigenvectors based on the training data so as to reflect a normal distribution.

For the training of the diffusion model, we split each dataset into 90% train and 10% test, and we train the Spectral Diffusion on the whole dataset for 100k epochs, using early stopping on the reconstruction loss. We performed a grid search on the number of layers between 6, 9 and 12, and selected the best model according to the degree metric computed from the graphs reconstructed directly from the eigenvectors/values and the graphs of the training set. The sampling has been done using DDIM with 200 steps. Moreover, we generate each sample 4 times and keep the one with the lower deviation from orthogonality.

For the training of the Graph Predictor, we used the same splits of the Spectral Diffusion, and trained for 100k epochs. We performed early stopping by comparing the degree distribution of the generated graphs with the training graphs. We used 6 PPGN layers and 3 PPGN layers for the Graph Predictor and the discriminator network respectively, except for QM9 in which also the Graph Predictor is composed of three layers. For QM9, we let the Graph Predictor to generate also edge features, similarly to Martinkus et al. (2022).

For all datasets, following the observations in Appendix E, we train both Spectral Diffusion and Predictor on the 16 smallest and 32 largest eigenpairs and select the final model according to the best average metrics on the validation set.

In order to guarantee the reproducibility of both our model architecture and results, we have made our code accessible on an online public repository<sup>2</sup>.

## E NUMBER OF EIGENVECTORS

To evaluate which part of the spectrum is more relevant and the proper number of eigenvectors to use, we performed an experiment. We trained our model focusing on either the smallest eigenvalues (Smallest) or the largest ones (Largest), while gradually increasing the corresponding number of eigenvectors taken into consideration. The results obtained from two synthetic datasets, Planar and SBM, are shown in Figure 7. Regarding the optimal number of eigenvectors, it appears that too many eigenvectors do not yield the best results, either considering low or high frequencies. Specifically, in the case of the Planar dataset, both smaller and larger eigenvalues exhibit the best performance with 16 eigenvectors. However, for SBM, while the optimal count for lower frequencies remains at 16, for higher frequencies, it increases to 32. These results are not entirely surprising, considering the inherent trade-off between the diffusion model’s capability to manage high-dimensional data and the quantity of information (number of eigenvectors) accessible to the Predictor. All in all, it should be noted that the selection of the number of eigenvectors can generally be regarded as a model hyperparameter for optimization, acknowledging its potential dependence on the specific dataset.

Building on the findings outlined above, in our experiments we employed the 32 largest eigenvalues and the 16 smallest eigenvalues - and their corresponding eigenvectors - for all datasets, except for the community-small dataset, for which we utilized the top 8 largest/smallest eigenvalues, and QM9, for which we used the full set of eigenpairs.

<sup>2</sup>Anonymized version <https://anonymous.4open.science/r/grasp-D237/>

918  
919  
920  
921  
922  
923  
924  
925  
926  
927

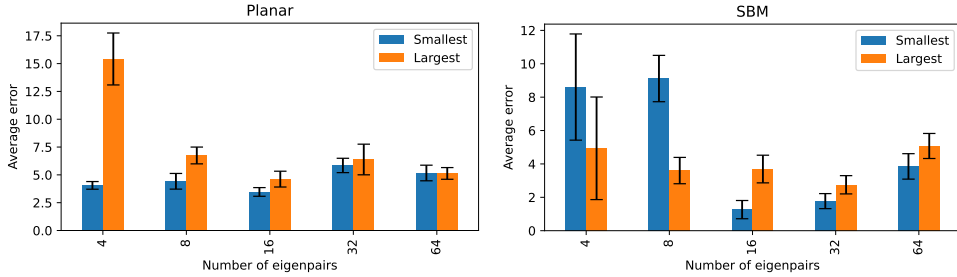


Figure 7: Performance analysis with varying numbers of eigenpairs and different spectrum parts, for the SBM (left) and Planar (right) datasets. The average error represents the mean degradation of all metrics between the generated graphs and the training set. We report both the mean and the standard deviation as error bars on 10 generations of 200 graphs. Specifically, we consider the Degree, Cluster, and Spectral metrics. For each metric, the degradation is computed as the ratio between (1) the MMD value computed between the generated graphs and the training graphs and (2) the MMD computed between the test graphs and the training graphs. A value of 1 indicates that the generated graphs exhibit the same statistical difference wrt the training graphs as the test set graphs do. The ratios computed for each metric are then averaged to get a single value indicating the quality of the generation.

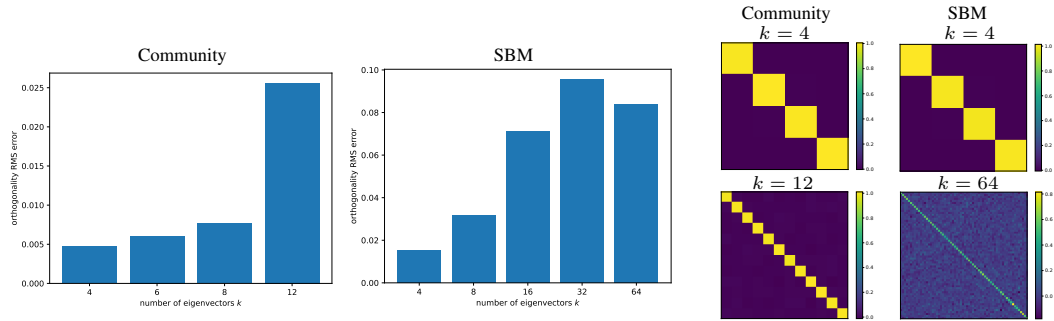
928  
929  
930  
931  
932  
933  
934  
935  
936  
937

## F EIGENVECTORS ORTHOGONALITY STUDY

938  
939  
940  
941

We conducted some experiments to provide both quantitative and qualitative analyses of the orthogonality behavior of the generated eigenvectors. In Figure 8 (left), we show how the generated eigenvectors deviate from forming an orthonormal basis. Here we vary the number of generated eigenvectors between 4 and 12 for Community, and between 4 and 64 for SBM. This choice reflects the fact that the graphs in the Community dataset have between 12 and 20 nodes, while in the case of SBM we observed that using more than 64 eigenvectors appears to lead to a degradation in performance (see Figure 8). As expected, increasing the number of generated eigenvectors introduces greater deviations from orthogonality, which aligns with our findings in Appendix E. In Figure 8 (right), we provide qualitative examples by comparing the generated eigenvectors with those computed from the adjacency matrix predicted by the PPGN. We can observe that in simpler datasets, such as the Community dataset, the eigenvectors are perfectly aligned. In more challenging datasets, such as SBM, while the alignment is not exact, the overall correspondence remains good and significant.

942  
943  
944  
945  
946  
947  
948  
949  
950  
951  
952  
953  
954  
955  
956  
957



958  
959  
960  
961  
962  
963  
964  
965  
966  
967  
968  
969  
970  
971

Figure 8: **Left:** the two bar plots show the deviation of the eigenvectors generated by GGSD from an orthonormal basis on two datasets for different numbers of eigenpairs. The deviation from orthogonality is computed as the average root mean squared difference of the inner product of the eigenvectors with the identity matrix, i.e.  $RMS(\tilde{\Phi}_0) = (\frac{1}{k^2} \mathbf{1}(\tilde{\Phi}_0^T \tilde{\Phi}_0 - \mathbf{I})^2 \mathbf{1}^T)^{\frac{1}{2}}$ , with  $\cdot^2$  being the elementwise square operator and  $k$  the number of eigenvectors. **Right:** Qualitative results showing the inner product of the generated eigenvectors.

$k$	1	2	3	4	5	6	7	8	9	10	11	12	13	14	15	16
SBM	1.11	2.54	3.62	4.88	6.65	6.88	7.11	7.42	7.51	7.75	7.47	7.84	7.76	7.85	8.26	8.13
Community	1.09	2.97	3.41	4.18	4.71	5.46	5.77	6.13	6.46	6.79	6.87	7.54	-	-	-	-

Table 6: Average Dirichlet energy computed on 500 generated graphs from the SBM and Community datasets, trained on the lower part of the spectrum (smaller eigenvalues).

The two experiments described above demonstrate that the generated eigenvectors exhibit the smoothness property and are often very similar, sometimes nearly identical, to the eigenvectors computed from the final predicted graph. To further investigate this, we computed the Dirichlet energy of the generated approximate eigenvectors on the final generated graph. We observed a consistent pattern, with the energy increasing as the eigenvalues grow larger. In Table 6, we report the average Dirichlet energy computed from 500 generated graphs in the SBM and Community datasets. We exclude the first eigenvector ( $\lambda = 0$ ) from the analysis, as it does not contribute to the reconstruction of the Laplacian, and the diffusion process is trained only on non-zero eigenvalues.

## G RUNTIME COMPARISON

Table 7: For each dataset, every method generates 100 graphs. We report the total generation time in seconds.

	Planar	SBM	Comm.	Proteins	QM9
GraphRNN	3.30	4.19	3.16	<b>16.87</b>	—
GRAN	8.58	48.43	2.90	205.47	—
DiGress	859.64	3882.30	70.49	OOM	68.11
<b>GSMD</b>	10.71	31.51	9.74	160.09	—
GDSS	81.10	160.88	456.30	3177.03	<u>1.32</u>
SPECTRE	<b>1.71</b>	<b>3.63</b>	<b>0.72</b>	OOM	<b>0.06</b>
<b>GGSD</b>	9.51	18.63	4.41	<u>124.07</u>	2.50

Table 7 shows the total generation time (in seconds) for our method and the baseline methods across the datasets analyzed in this paper. For a fair comparison, we generated 100 graphs for each dataset and method. These experiments were conducted on a computer equipped with an AMD Ryzen 7 3700X processor, 64GB of RAM, and an NVIDIA RTX 3070 8GB graphics card. We achieve a significant speedup compared to DiGress, thus showing that we are able to overcome the computational bottleneck of diffusion-based methods which, unlike **GGSD**, work on a diffusion space that is quadratic in the number of nodes of the graph. Additionally, our hardware configuration could not register the time for large datasets like Proteins due to their space complexity. While our method outperforms GDSS in terms of speed, it is less efficient than simpler algorithms such as GRAN and GraphRNN.

## H STABILITY OF THE SPECTRAL DECOMPOSITION OF THE GRAPH LAPLACIAN

In the spectral graph theory literature, the instability of the Laplacian has become a true-ism. Yet, this claim requires further qualification as several spectral approaches have shown to be robust even under severe deformation Rodolà et al. (2017). In general, random structural perturbation can cause major topological changes which will reflect on the eigenvectors and eigenvalues of the Laplacian quite dramatically, but it strongly depends on the location of the actual perturbation, and it is linked with small gaps in the eigenvalues.

From spectral perturbation theory, we note that under a perturbation  $\mathcal{E}$ , as long as the eigenvalues are and remain distinct, the eigenvalues of the perturbed Laplacian  $\tilde{\mathbf{L}} = \mathbf{L} + \mathcal{E}$  are perturbed by a

1026 quantity

$$1027 \Delta\lambda_i \approx \phi_i^T \mathcal{E} \phi_i, \quad (8)$$

1028 while the eigenvectors are perturbed by  $\Delta\Phi \approx \Phi\mathbf{B}$ . Here the matrix  $\mathbf{B} = (b_{ij})$  is defined as:

$$1030 b_{ij} = \frac{\phi_i^T \mathcal{E} \phi_j}{\lambda_j - \lambda_i}. \quad (9)$$

1031  
1032  
1033 As a consequence, the mixing can become large even for small perturbations if the gap between  
1034 the eigenvalues is small, and in general only eigenvectors with close eigenvalues will mix in a  
1035 significant way. All this being said, this characterizes what happens when we perturb the graph,  
1036 which is not what is happening here. By recreating the spectrum through a stable diffusion process,  
1037 the perturbation is in the spectrum, and, in general, small perturbations of the spectrum do not cause  
1038 major topological changes in the structure (which, as we said, are associated with large spectral  
1039 variations). Let us say that the eigenvectors are perturbed by a factor of  $\Delta\Phi$  and the eigenvalues by  
1040 a factor of  $\Delta\Lambda$ , then the reconstructed Laplacian is

$$1041 \tilde{\mathbf{L}} = (\Phi + \Delta\Phi)(\Lambda + \Delta\Lambda)(\Phi + \Delta\Phi)^T = \Phi\Lambda\Phi^T + \underbrace{\Phi\Delta\Lambda\Phi^T + \Phi\Lambda\Delta\Phi^T + \Delta\Phi\Lambda\Phi^T}_{\text{I order error terms}} +$$

$$1042$$

$$1043 \underbrace{\Phi\Delta\Lambda\Delta\Phi^T + \Delta\Phi\Delta\Lambda\Phi^T + \Delta\Phi\Lambda\Delta\Phi^T}_{\text{II order error terms}} + \underbrace{\Delta\Phi\Delta\Lambda\Delta\Phi^T}_{\text{III order error term}}, \quad (10)$$

1044  
1045  
1046 which varies smoothly with noise and does not have elements at the denominator that force the terms  
1047 to explode. Indeed, we have not observed topological instabilities in any of the datasets considered  
1048 in this study.

1049  
1050  
1051  
1052  
1053  
1054  
1055  
1056  
1057  
1058  
1059  
1060  
1061  
1062  
1063  
1064  
1065  
1066  
1067  
1068  
1069  
1070  
1071  
1072  
1073  
1074  
1075  
1076  
1077  
1078  
1079